Elliptic Gaussian optical vortices

V. V. Kotlyar, A. A. Kovalev, and A. P. Porfirev
Image Processing Systems Institute of the RAS – Branch of the FSRC "Crystallography and Photonics" of the RAS, Samara 443001, Russia and S.P. Korolyov Samara National Research University, Samara 443086, Russia
(Received 14 March 2017; published 1 May 2017)

We analyze an elliptic optical vortex embedded into a Gaussian beam. Explicit closed expressions for the complex amplitude and normalized orbital angular momentum (OAM) of such a beam are derived. The resulting elliptic Gaussian vortex (EGV) is shown to have a fractional OAM whose maximal value equal to the topological charge n of a conventional Gauss vortex is attained for a zero-ellipticity vortex. As the beam propagates, the major axis of the intensity ellipse in the beam cross section rotates, making the angle of 90° between the initial plane and the focal plane of a spherical lens. On the major axis of the intensity ellipse, there are n intensity nulls of the EGV, with the distance between them varying with propagation distance and varying ellipticity. The distance between the intensity nulls is found to be maximal in the focal plane for a given ellipticity. For zero ellipticity, all intensity nulls get merged into a single n-times degenerate on-axis intensity null. The experimental results are in good agreement with theory.

DOI: 10.1103/PhysRevA.95.053805

I. INTRODUCTION

Optical vortices that are devoid of radial symmetry and carry a fractional orbital angular momentum (OAM) have been studied intensively in the last several years. This interest is due to the fact that optical vortices with fractional OAM have found use in quantum computing for generating the entanglement of the orbital angular momentum states of photon pairs [1–3]. For example, in Ref. [1] obtaining the fractional OAM was done by shifting the "fork" hologram with the topological charge $n = 1$ from the center of the illuminating Gaussian beam. The fact that such shift leads to the fractional OAM of an optical vortex is described in Ref. [4]. In this way, ultrahigh security of quantum communication lines can be achieved.

An optical vortex with fractional OAM can be generated using a variety of techniques. For instance, this can be done by an off-axis shift of a Gaussian beam from the center of a spiral phase plate (SPP) [4]. Another possibility involves generating asymmetric optical vortices with a crescent-shaped intensity pattern [5,6]. However, in this case the microparticle trapped in the beam moves on an open trajectory. It would be of interest to study a situation when the OAM is fractional and the intensity curve in the transverse plane of the vortex is closed. The simplest approach is based on generating an elliptic optical vortex. Transformation of an optical vortex via introducing varying ellipticity was discussed in Ref. [7], which was a follow-up of earlier studies of elliptic optical vortices [8,9]. However, the OAM of elliptic vortices was not considered in Refs. [7–9]. Topics dealt with in the present article are most close to those discussed in Ref. [10], which studied an elliptic Hermite-Gaussian vortex, calculating the corresponding OAM and finding it to be fractional. For such a beam to be practically generated, an elliptic Gaussian beam needs to be incident on an amplitude-phase optical element. However, combining the required amplitude and phase in a single element is a challenging task. There are also works where more complicated elliptical Gaussian vortices with fractional OAM were studied, including general-form elliptic beams (EB) [11], Ince-Gaussian (IG) beams [12], helical Ince-Gaussian (HIG) beams [13], Ince-Gaussian beams in a parabolic gradient-index medium [14], Hermite-Laguerre-Gaussian (HLG) beams [15], Mathieu [16] beams, and Lommel [17] modes. It was shown experimentally in Ref. [18] that HIG beams allow generation of OAM-entangled pairs of photons, while in Ref. [19] it was shown theoretically that HIG beams have a fractional OAM, which changes nonmonotonically with increase of the ellipticity parameter. We note that it was shown numerically in Ref. [16] that Mathieu beams have a fractional OAM which changes with the ellipticity parameter the same way as the OAM of HIG beams, i.e., it decreases at first and then increases. We note also that it was shown in Ref. [20] that cylindrical lens allows generating an elliptical noncanonical vortex, which can change the sign of its topological charge on propagation in space. It was demonstrated experimentally in Ref. [21] that by using spiral phase plates with a fractional topological charge it is possible to generate entangled pairs of photons with the fractional OAM. Note that all above-mentioned elliptical beams have the fractional OAM, but closed-form expressions for the fractional OAM are only in Refs. [4,10,15,17]. In Refs. [16,19], there are expressions for the OAM in the form of an infinite series.

In this work, we study simple elliptical Gaussian optical vortices (EGVs). We derive a relationship to describe the OAM of a Gaussian beam that is embedded with an elliptic optical vortex with n-times degenerate on-axis intensity null (at the Gaussian beam's center). As distinct from Ref. [10], in which the OAM increased with increasing ellipticity of the Gaussian beam, we discuss a situation where the OAM decreases with increasing ellipticity of the embedded optical vortex. Also, note that the optical vortex discussed in Ref. [10] was found to preserve its shape upon propagation up to a scale, with the transverse intensity pattern defined by an ellipse with n isolated intensity nulls. In this work, while featuring a rotating elliptic transverse intensity pattern, the major-axis intensity nulls of the vortex beam are only found in the focal plane of a spherical lens.

We now briefly compare the above-mentioned various types of elliptical vortex beams. IG [12] and HIG beams [13] differ from the HLG beams [15], since the HLG beams tend in the limiting cases to the conventional Hermite-Gaussian (HG) or Laguerre-Gaussian (LG) beams, while the IG beams in the

limiting cases tend only to the HG beams and HIG beams tend only to the LG beams. In addition, with increasing ellipticity OAM of the HIG beams changes nonmonotonically [19], while OAM of the HLG beams monotonically decreases toward zero [15]. The EGV beams considered here differ both from HIG beams and from HLG beams, since first they have different dependence of the OAM on the ellipticity parameter, and second, the EGV beams are not modes and change their shape on propagation in space. In the center of the initial plane, EGV has an n-fold degenerate intensity null, while in any other transverse plane there are n isolated intensity nulls, lying on a straight line, which rotates (as the whole beam) on propagation. Since the elliptic beams [11] are space modes and at some parameters they reduce to the IG beams [12] and to the Mathieu beams [16], they also differ from the EGV beams. In addition, yet another difference of these beams is that EB, IG, and Mathieu beams are decomposed into an infinite series of the LG modes [22]; the HLG beam is a finite sum of the HG modes [15], while the EGV is a finite sum of the LG beams with different n. We also note that solutions of the paraxial equation as a product of the Ince polynomials and the Gaussian function, obtained by separation of variables in the elliptical coordinates, have been known in mathematics for a long time [23].

II. COMPUTATION OF THE ORBITAL ANGULAR MOMENTUM

Assume an isolated n-times degenerate elliptic intensity null at the origin, described as

$$T(x,y) = (\alpha x + iy)^n, \tag{1}$$

where n is the integer topological charge of the optical vortex, α is a dimensionless parameter that defines the ellipticity of the intensity null: if $\alpha < 1$, the major axis is on the x axis, if $\alpha > 1$ – on the y axis, if $\alpha < 0$, the vortex phase rotates clockwise, if $\alpha > 0$ – anticlockwise.

Let the intensity null (1) be embedded into the waist of a Gaussian beam, so that the complex amplitude of the light field in the initial plane takes the form

$$E(x,y,z=0) = (\alpha x + iy)^n \exp\left(-\frac{x^2+y^2}{2w^2}\right), \tag{2}$$

where w is the waist radius of the Gaussian beam. We shall seek the OAM and power of the paraxial field using well-known formulas [5,7]:

$$J_z = \mathrm{Im}\left\{\int_{-\infty}^{\infty}\int_{-\infty}^{\infty} \bar{E}(x,y)\left(x\frac{\partial}{\partial y} - y\frac{\partial}{\partial x}\right)E(x,y)dxdy\right\}, \tag{3}$$

$$W = \int_{-\infty}^{\infty}\int_{-\infty}^{\infty} \bar{E}(x,y)E(x,y)dxdy, \tag{4}$$

where Im is the imaginary part of a complex number and $\bar{E}$ is a conjugate complex amplitude. For the field in (2), Eqs. (3) and (4) are rearranged to

$$J_z = \alpha n \int_{-\infty}^{\infty}\int_{-\infty}^{\infty} \exp\left(-\frac{x^2+y^2}{w^2}\right) \times(\alpha^2x^2+y^2)^{n-1}(x^2+y^2)dxdy, \tag{5}$$

$$W = \int_{-\infty}^{\infty}\int_{-\infty}^{\infty} \exp\left(-\frac{x^2+y^2}{w^2}\right)(\alpha^2x^2+y^2)^n dxdy. \tag{6}$$

From (5) and (6) it follows that if the intensity null has zero ellipticity ($\alpha = 1$), we obtain a well-known normalized OAM equal to the topological charge of the vortex [24]:

$$\frac{J_z}{W} = n. \tag{7}$$

If $\alpha = -1$, Eq. (7) has the opposite sign: $J_z/W = -n$. The integrals in (5) and (6) can be calculated based on the integral

$$I_m = \int_{-\infty}^{\infty}\int_{-\infty}^{\infty} \exp\left(-\frac{x^2+y^2}{w^2}\right)(\alpha^2x^2+y^2)^m dxdy, \tag{8}$$

because the OAM in (5) and power in (6) are connected with (8) via simple relations:

$$J_z = -\alpha n \frac{\partial}{\partial(w^{-2})} I_{m=n-1}, \quad W = I_{m=n}. \tag{9}$$

Integral (8) is calculated using an expansion in terms of Newton binomials

$$(\alpha x + iy)^n = \sum_{l=0}^{n} \frac{n!}{l!(n-l)!}(\alpha x)^l (iy)^{n-l}, \tag{10}$$

and a simple integral

$$\int_{-\infty}^{\infty} x^{2l}\exp(-px^2)dx = \sqrt{\pi}2^{-l}(2l-1)!!\,p^{-(2l+1)/2}, \tag{11}$$

with the factorial $(2l-1)!!$ taken over odd integer numbers. Applying (10) and (11) to (8) and accounting for (9), Eqs. (5) and (6) are rearranged to

$$J_z = \frac{\pi\alpha n^2 w^{2n+2}}{2^{n-1}} A_{n-1}, \quad W = \frac{\pi w^{2n+2}}{2^n} A_n, \tag{12}$$

where

$$A_n = \sum_{l=0}^{n} \frac{n!(2l-1)!!(2n-2l-1)!!}{l!(n-l)!}\alpha^{2l}. \tag{13}$$

From (12), the normalized OAM of the field in (2) takes the form

$$\frac{J_z}{W} = \frac{2\alpha n^2 A_{n-1}}{A_n}. \tag{14}$$

Considering that it is difficult to draw specific conclusions from (14), below we give simplified expressions for the

normalized OAM with the topological charges $n = 1,2,3$:

$$\frac{J_z}{W}|_{n=1} = \frac{2\alpha}{1+\alpha^2}, \tag{15}$$

$$\frac{J_z}{W}|_{n=2} = \frac{8\alpha(1+\alpha^2)}{3+2\alpha^2+3\alpha^4}, \tag{16}$$

$$\frac{J_z}{W}|_{n=3} = \frac{6\alpha(3+2\alpha^2+3\alpha^4)}{5+3\alpha^2+3\alpha^4+5\alpha^6}. \tag{17}$$

From (15)–(17) the OAM of optical vortex (2) is seen to be fractional and smaller than the topological charge n both at $\alpha < 1$ and at $\alpha > 1$. Hence, yet omitting a proof we can suggest that at $\alpha > 0$

$$\frac{J_z}{W} = \frac{2\alpha n^2 A_{n-1}}{A_n} \leqslant n. \tag{18}$$

It can be shown also that the normalized OAM can be expressed more compactly by using the Legendre polynomials:

$$\frac{J_z}{W} = n\frac{P_{n-1}(s)}{P_n(s)}, \tag{19}$$

where $s = (1+\alpha^2)/(2\alpha)$. Since $P_n(1) = 1$ for any n, then for circular Gaussian vortex ($\alpha = 1$) we obtain the well-known property that the normalized OAM equals the topological charge. Using the properties of the Legendre polynomials [25] it can be shown that $P_n(\xi) > P_{n-1}(\xi)$ at any $\xi > 1$. Since the value of s is always not less than unity, this inequality proves the inequality (18). For comparison, we note that the OAM (19) as a ratio of the Legendre polynomials is not a unique case. For example, OAM in Ref. [4] can be expressed as a ratio of the Laguerre polynomials, although the optical vortex in Ref. [4] has a crescent shape instead of being elliptical. From Eq. (19), it follows that with increasing ellipticity parameter the OAM decreases and tends to zero. We note that the OAM of HLG beams [15] and of asymmetric vortex Gaussian beams [4] also decreases (although in a different way) toward zero with increasing ellipticity. With increasing ellipticity, the OAM of the elliptic HIG beams [19] and of the Mathieu beams [16] initially decreases and then grows (or only decreases). Decrease of the OAM [16,19] is related to increasing distance between the intensity nulls with unit topological charge, while increase of the OAM is related to new optical vortices appearing in the beam. We note, however, that in contrast to the Lommel modes [17], whose OAM can grow to infinity, the OAM of the HIG beams can grow to some limiting value. Indeed, the HIG (p,m) beams [13,19] in the limit reduce to a linear combination of two HG beams: HG $(p-m,m) \pm i$ HG $(p-m-1,m+1)$. It was shown in Ref. [26] that the OAM of such sum of two HG modes equals the maximal index, for example $p-m$. Therefore, the OAM of the HIG beam starts from the integer value m and with increasing ellipticity asymptotically decreases if $p-m < m$, or asymptotically increases if $p-m > m$.

Note that the equality in (18) is attained at $\alpha = 1$. Physics behind the decrease of OAM resulting from the replacement of a conventional rotationally symmetric vortex with the elliptic vortex (1) may be as follows. The OAM density is higher in areas with larger curvature of the intensity ellipse in the cross section of the EGV beam. However, in areas where the optical vortex is elongated the amplitude of the Gaussian beam is lower so that the "elongated" optical vortex fragments contribute less to the total OAM (18). From (15)–(17), we can infer that at definite vales of α the OAM becomes equal to an integer $m < n$. Therefore, varying the ellipticity of the isolated intensity null (1) α from 0 to 1, it is possible to obtain an optical vortex with any normalized OAM in the range from 0 to n.

III. COMPUTING THE FIELD COMPLEX AMPLITUDE

At an arbitrary distance z, the field's complex amplitude in (2) can be calculated using a Fresnel transform. Field (2) can be complemented by the transmittance of a thin spherical lens in the paraxial approximation:

$$F(x,y) = \exp\left[-\frac{ik}{2f}(x^2+y^2)\right], \tag{20}$$

where f is the focal length of the thin lens and k is the wave number. Then, after passing the spherical lens (20), the complex amplitude of the elliptic Gaussian vortex (2) takes the integral form:

$$E(\xi,\eta,z) = \left(\frac{-ik}{2\pi z}\right)\int_{-\infty}^{\infty}\int_{-\infty}^{\infty} E(x,y,z=0)F(x,y) \times \exp\left[\frac{ik}{2z}\{(x-\xi)^2+(y-\eta)^2\}\right]dxdy. \tag{21}$$

Integral (21) can be calculated as the sum in (10) and two reference relationships [25]:

$$\int_{-\infty}^{\infty} x^m \exp(-Ax^2 - Bx)dx = \sqrt{\pi}\left(\frac{i}{2}\right)^m A^{-(m+1)/2}\exp\left(\frac{B^2}{4A}\right)H_m\left(\frac{iB}{2\sqrt{A}}\right), \tag{22}$$

$$\sum_{l=0}^{m}\frac{m!t^l}{l!(m-l)!}H_l(X)H_{m-l}(Y) = (1+t^2)^{m/2}H_m\left(\frac{tX+Y}{\sqrt{1+t^2}}\right), \tag{23}$$

where $H_m(x)$ is a Hermite polynomial. Then, Eq. (21) reduces to ($\alpha > 1$)

$$E(\xi,\eta,z) = \left(\frac{-1}{2}\right)^n\left(\frac{-ik}{2z}\right)\left(\frac{\sqrt{2}w}{1+iz_0/z}\right)^{n+2} \times \exp\left[-\frac{\xi^2+\eta^2}{P^2}+\frac{ik}{2S}(\xi^2+\eta^2)\right] \times(1-\alpha^2)^{n/2}H_n(Q(R+iI)), \tag{24}$$

where

$$P = \frac{\sqrt{2}wz}{z_0}\sqrt{1+\frac{z_0^2}{z_1^2}},$$

$$S = z\left\{1+\left[\frac{z}{z_1}\left(1+\frac{z_1^2}{z_0^2}\right)\right]^{-1}\right\}^{-1},$$

$$z_1 = \frac{zf}{z-f}, \quad z_0 = kw^2,$$

$$Q = \frac{kw}{\sqrt{2}z}(\alpha^2-1)^{-1/2}\left(1+\frac{z_0^2}{z_1^2}\right)^{-1/4},$$
$$I = \eta\cos\psi - \alpha\xi\sin\psi,\ R = -\alpha\xi\cos\psi - \eta\sin\psi,$$
$$\psi = \frac{1}{2}\arctan\left(\frac{z_0}{z_1}\right). \quad (25)$$

From (24) and (25) it follows that the argument of the Hermite polynomial takes real values only on a straight line in the transverse plane, satisfying the equation

$$\eta = \alpha\xi\tan(\psi). \quad (26)$$

From (26) it follows that at $z = 0$, $z_1 = 0$, and $\psi = \pi/4$, i.e., the straight line (26) is inclined (tangent of inclination angle equals α). At $z = f$, $z_1 \to \infty$, and $\psi = 0$, which means that the line is horizontal. At other distances, $0 < z < f$, the line (26) is gradually rotated from the inclined to horizontal position. It is on the line of real-valued arguments that the roots of the Hermite polynomial [intensity nulls of field (24)] are found. Having equated the real part of the Hermite polynomial in (24) to the root value γ_n, where $H_n(\gamma_n) = 0$, and taking account of (26), we derive an equation for the coordinates of the intensity nulls on the horizontal ξ axis [the intensity null coordinates on the vertical axis follow from (26)]:

$$\xi_n = -\frac{\sqrt{2}\gamma_n z\sqrt{\alpha^2-1}\left(1+\frac{z_0^2}{z_1^2}\right)^{1/4}}{\alpha kw}\cos(\psi). \quad (27)$$

Equation (27) suggests that at $\alpha = 1$, function (24) has a single intensity null, $\xi_n = 0$. At small z and $\alpha > 1$, the intensity nulls (27) are located close to each other. The maximal spacing between the nulls (27) is in the lens focus at $z = f$:

$$\xi_n = -\frac{\sqrt{2}\gamma_n f\sqrt{\alpha^2-1}}{\alpha kw}. \quad (28)$$

From (28) it can be inferred that the spacing between the nulls of field (24) located on a horizontal line in the focal plane of spherical lens (20) depends on the optical vortex's ellipticity α. At $\alpha = 1$, the spacing between the intensity nulls equals zero, whereas at $\alpha \to \infty$ it is maximal, becoming equal to

$$\xi_n = -\frac{\sqrt{2}\gamma_n f}{kw}. \quad (29)$$

We note that increase of the distance between the intensity nulls with increasing ellipticity α and at the fixed Gaussian beam waist radius leads to the decrease of the OAM [26].

It is worth noting that by choosing the inverse value $\beta = 1/\alpha$ as the ellipticity of the optical vortex (1), Eq. (28) is rearranged to

$$\xi_n = -\frac{\sqrt{2}\gamma_n f\sqrt{1-\beta^2}}{kw}, \quad (30)$$

from which it follows that at $\beta = 1$ the spacing between the intensity nulls equals zero (i.e., there is just one intensity null at the origin in the lens focal plane), whereas at $\beta = 0$ the spacing between the nulls is maximal and defined by (29).

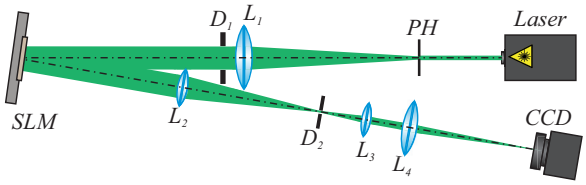

FIG. 1. An experimental setup: L is a solid-state laser ($\lambda = 532$ nm), PH is a 40-μm pinhole, L_1, L_2, L_3, and L_4 are lenses with focal lengths $f_1 = 250$ mm, $f_2 = 350$ mm, $f_3 = 150$ mm, and $f_4 = 500$ mm, D_1 and D_2 are diaphragms, *SLM* is a spatial light modulator PLUTO VIS, and *CCD* is a video-camera LOMO TC-1000.

IV. EXPERIMENTS ON GENERATING AN ELLIPTIC GAUSSIAN BEAM

In the experiment, a linearly polarized Gaussian beam of waist diameter $2w = 2.7$ mm was near-orthogonally incident on an elliptic spiral phase plate with the transmittance

$$V(r,\varphi) = \exp(in\varphi), \quad (31)$$

where $\varphi = \arctan[(c_y y)/(c_x x)]$. The ratio $c_y/c_x = \beta = 1/\alpha$ was taken to equal 0.1; 0.2; 0.4; 0.6; 0.8; and 1.0. Note that although function (31) is different from function (1), both optical vortices have the same topological charge, given the same n and α. This makes both vortices behave in a similar way.

An experimental setup is shown in Fig. 1. A solid-state laser L ($\lambda = 532$ nm) was used as a light source, generating a fundamental Gaussian beam. The laser light was expanded and collimated by sequentially passing through a 40-μm pinhole PH and lens L_1 ($f_1 = 250$ mm), before hitting the display of a modulator *SLM* (PLUTO VIS, 1920 × 1080 resolution, and 8-μm pixel size). The diaphragm D_1 was utilized to single out the central bright ring from surrounding bright and dark rings resulting from diffraction by the pinhole. Then, using lenses L_2 ($f_2 = 350$ mm) and L_3 ($f_3 = 150$ mm) and diaphragm D_2 the phase-modulated laser beam reflected at the modulator's display was spatially filtered. Lens L_4 ($f_4 = 500$ mm) was used to focus the laser beam on the matrix of the charge-coupled-device camera LOMO TC 1000 (3.34 × 3.34-μm pixel size).

Shown in Fig. 2 are phase functions of the spiral phase plates with different ellipticity β and corresponding experimental and computed intensity distributions generated in the focus of lens L_4. The spiral phase plate carries a topological charge of $n = 1$. A minor deviation of the intensity distribution observed at $\beta = 1$ from a perfect ring is due to the minor deviation of the incident light from normal.

Figure 3 shows phase functions of the spiral plates with different ellipticity β and corresponding experimental and computed intensity distributions they generate in the focus of lens L_4. The SPP carries a topological charge of $n = 2$. A minor deviation of the resulting intensity distribution observed at $\beta = 1$ from a perfect ring is due to the minor deviation of the incident beam from normal.

Note that the relations (15)–(17) are invariant to the substitution of parameters: $\alpha \to \beta$. Hence, substituting in (16) β for α, we get the OAM of the optical vortices shown in Figs. 3(g)–3(l), as presented in Table I. From Fig. 3, the spacing between two adjacent intensity nulls is seen to

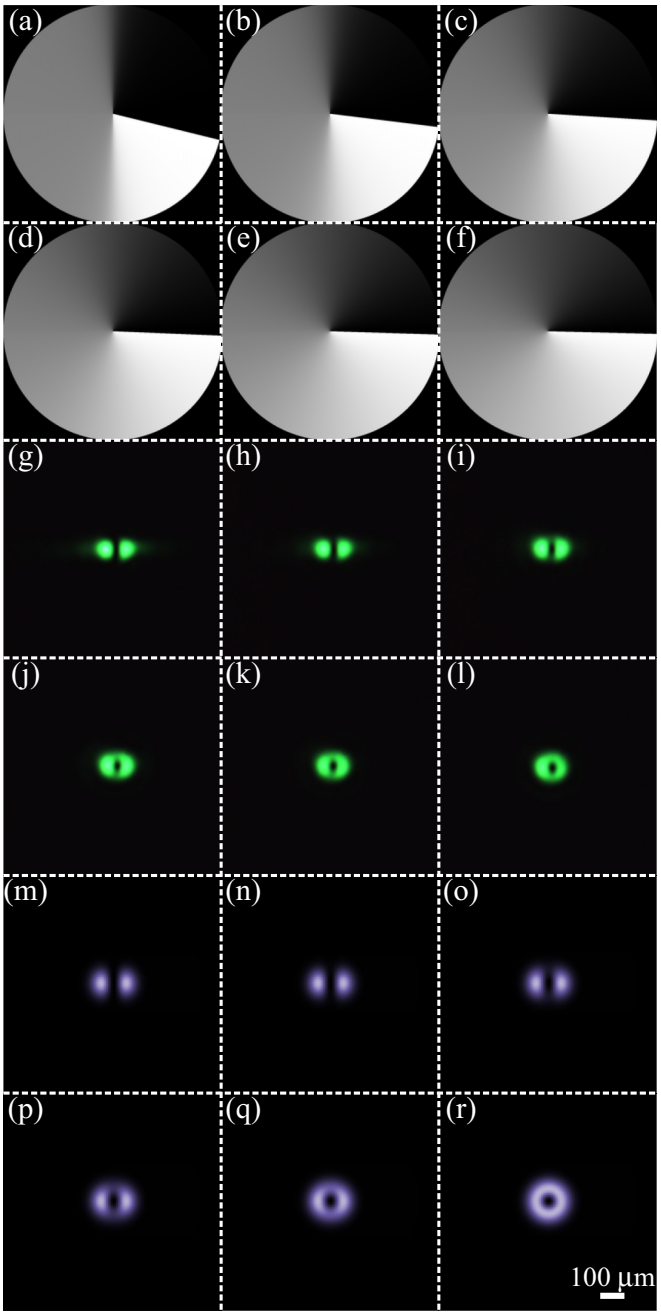

FIG. 2. (a)–(f) Phase functions of the optical elements; (g)–(l) corresponding experimental intensity distributions; and (m)–(r) computed intensity distributions in the focus of lens L_4 when using a SPP with $n = 1$ and the ratio β taking values of 0.1 (a), (g), (m); 0.2 (b), (h), (n); 0.4 (c), (i), (o); 0.6 (d), (j), (p); 0.8 (e), (k), (q); and 1.0 (f), (l), (r). The intensity patterns are 900 μm × 900 μm in size.

TABLE I. Normalized OAM derived from (16) and computed numerically for an elliptic Gaussian vortex with $n = 2$ and varying ellipticity β.

Fig. 3	(g)	(h)	(i)	(j)	(k)	(l)
β	0.1	0.2	0.4	0.6	0.8	1.0
J_z/W (theory)	0.26	0.53	1.11	1.56	1.91	2.00
J_z/W (comput.)	0.27	0.54	1.09	1.59	1.91	2.00

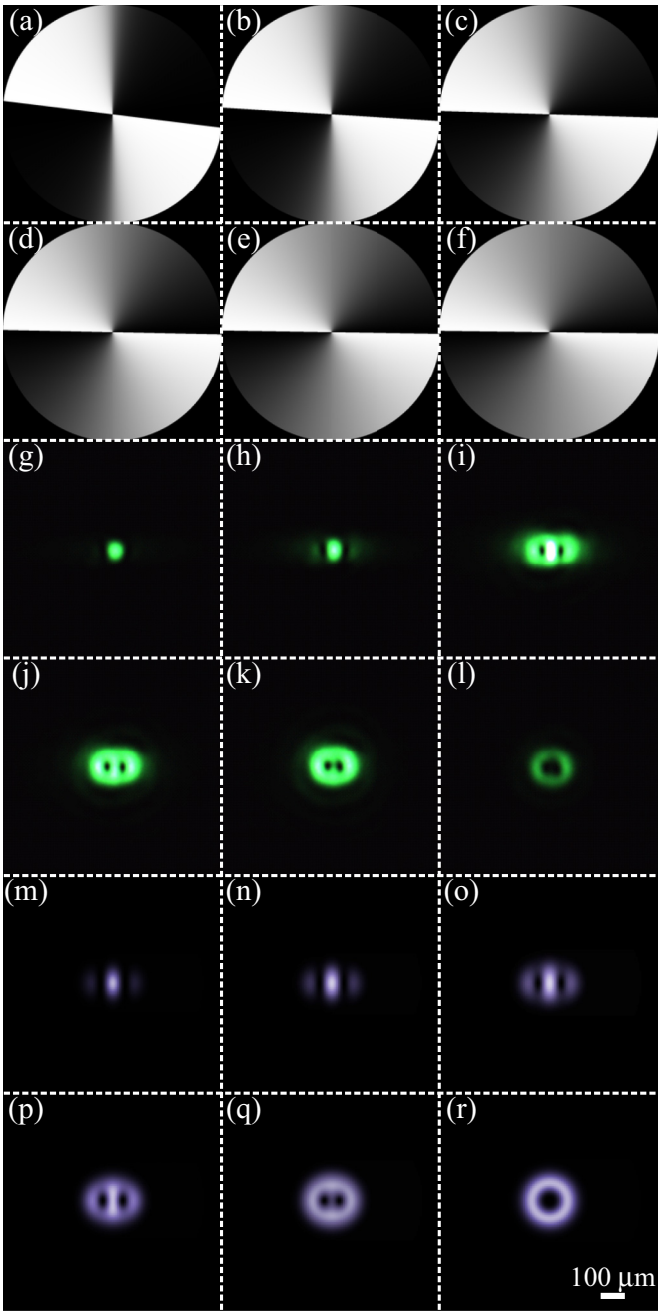

FIG. 3. (a)–(f) Phase functions of the elements; (g)–(l) corresponding experimental intensity distributions; and (m)–(r) computed intensity distributions in the focus of lens L_4 for a SPP with the topological charge $n = 2$ and with the ratio β taking values of 0.1 (a), (g), (m); 0.2 (b), (h), (n); 0.4 (c), (i), (o); 0.6 (d), (j), (p); 0.8 (e), (k), (q); and 1.0 (f), (l), (r). The intensity patterns are 900 μm × 900 μm in size.

decrease [according to (30)] from Fig. 3(g) to Fig. 3(l), while the OAM on the contrary increases from Fig. 3(g) to Fig. 3(l) (see Table I, row 3).

It is interesting that Table I suggests that in the range 0.2–0.4 there is a β value such that the elliptic beam has a unit OAM. Nonetheless, such an optical vortex has two intensity nulls in the lens focal plane rather than having a single null, which is the case with all similar optical vortices in Fig. 3.

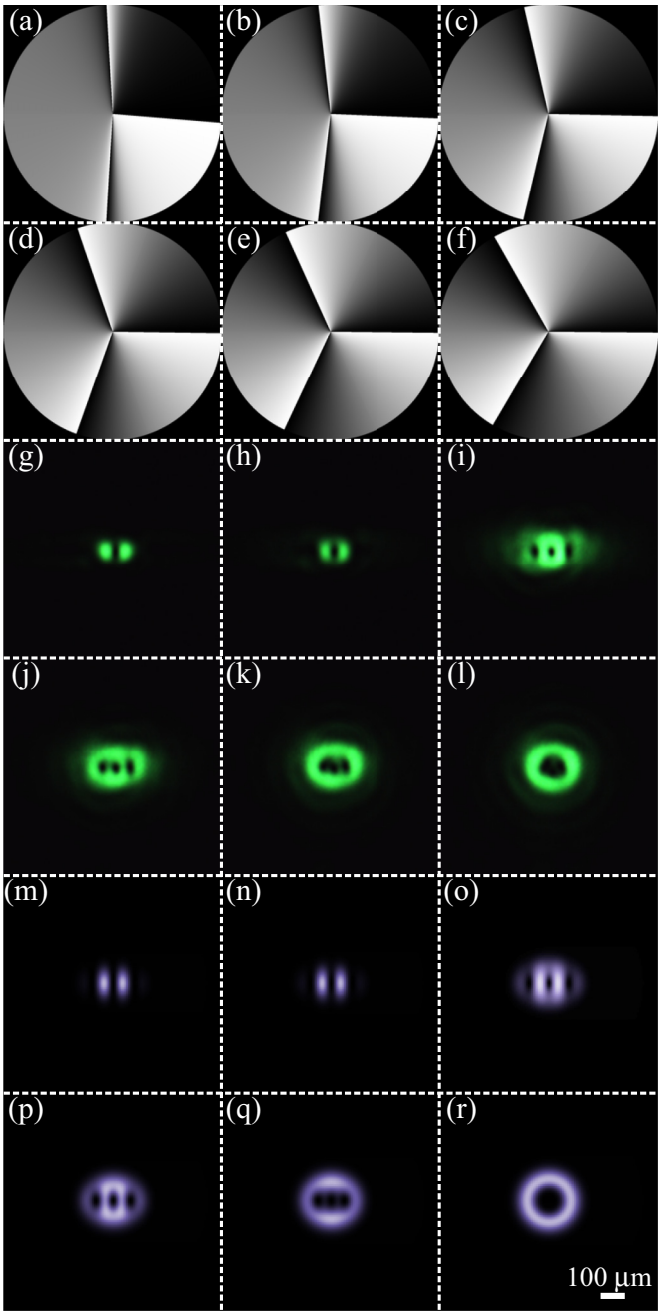

FIG. 4. (a)–(f) Phase functions of the elements; (g)–(l) corresponding experimental intensity distributions; and (m)–(r) computed intensity distributions in the focus of lens L_4 when using a SPP with $n = 3$ and with the ratio β taking values of 0.1 (a), (g), (m); 0.2 (b), (h), (n); 0.4 (c), (i), (o); 0.6 (d), (j), (p); 0.8 (e), (k), (q); and 1.0 (f), (l), (r). The intensity patterns are 900 μm × 900 μm in size.

Figure 4 depicts phase functions of the SPPs with different ellipticity β and corresponding experimental and computed intensity distributions generated in the focus of lens L_4. The SPP has $n = 3$. A minor deviation of the intensity distribution generated at $\beta = 1$ from a perfect ring is due to the minor deviation of the incident light from normal.

Table II gives values of the normalized OAM derived from (17) and computed numerically for an elliptic Gaussian beam with $n = 3$ and different values of β. Figure 4 shows that the spacing between three intensity nulls is decreasing [in accordance with (30)] from Fig. 4(g) to Fig. 4(l), while OAM on the contrary is increasing from Fig. 4(g) to Fig. 4(l) (see Table I, row 3). In Figs. 4(g) and 4(h) a single intensity null is clearly seen because two other intensity nulls are found in the Gauss beam's low-intensity region. The nulls are well discernible starting from Fig. 4(i). In Fig. 4(l), the three intensity nulls get merged, forming the intensity null of a conventional radially symmetric optical vortex.

TABLE II. Normalized OAM derived from (17) and computed numerically for an elliptic Gauss vortex with $n = 3$ and varying ellipticity β.

Fig. 3	(g)	(h)	(i)	(j)	(k)	(l)
β	0.1	0.2	0.4	0.6	0.8	1.0
J_z/W (theory)	0.36	0.72	1.47	2.20	2.97	3.00
J_z/W (comput.)	0.36	0.72	1.46	2.21	2.80	3.00

Figure 5 depicts phase functions of the SPP with varying ellipticity β and corresponding experimental and computed intensity distributions generated in the focus of lens L_4. The SPP has $n = 4$. A minor deviation of the intensity distribution generated at $\beta = 1$ is due to the minor deviation of the incident light from normal.

Four intensity nulls in the lens focus are clearly discernible only in Figs. 5(i) and 5(j). In Fig. 5(g), the nulls are not yet seen because they are located in the Gaussian beam's low-intensity region. In Fig. 5(h) just two intensity nulls can be seen, with the two others found in the low-intensity region. In Figs. 5(k) and 5(l) the situation is different: being located close to each other, the nulls are hardly discernible.

Figure 6 depicts intensity distributions of an elliptic Gauss vortex with the topological charge $n = 4$ and ellipticity $\beta = 0.6$ registered at different distances from the initial plane (prior to and behind the focal plane of lens L_4).

Figure 6 suggests that in compliance with (26), while remaining in quadrants II and IV, the major axis of the transverse intensity ellipse of the optical vortex rotates upon propagation, changing from the initial vertical to the horizontal position in the lens focal plane [Fig. 6(g)]. Vice versa, after passing the focus, the major axis of the intensity ellipse rotates from the horizontal to the vertical position, remaining in quadrants I and III. The tilt of the straight line in (26) changes its sign because of changing sign of the variable $z_1 = zf/(z - f)$ after passing the focus, leading to the change of sign of the angle $\psi = \arctan(z_0/z_1)/2$. In accordance with (27), the spacing between four intensity nulls on the major axis of the intensity ellipse increases, reaching its maximum (28) in the lens focal plane [Fig. 6(g)]. Because of this, four intensity nulls are clearly discernible just in the focal plane in Fig. 6(g). After passing the focus, as the spacing decreases, the nulls become hardly discernible.

V. CONCLUSION

Summing up, the following results have been obtained. Explicit closed relationships for the complex amplitude and normalized OAM of a conventional Gaussian beam implanted with an elliptic optical vortex with an n-times degenerate

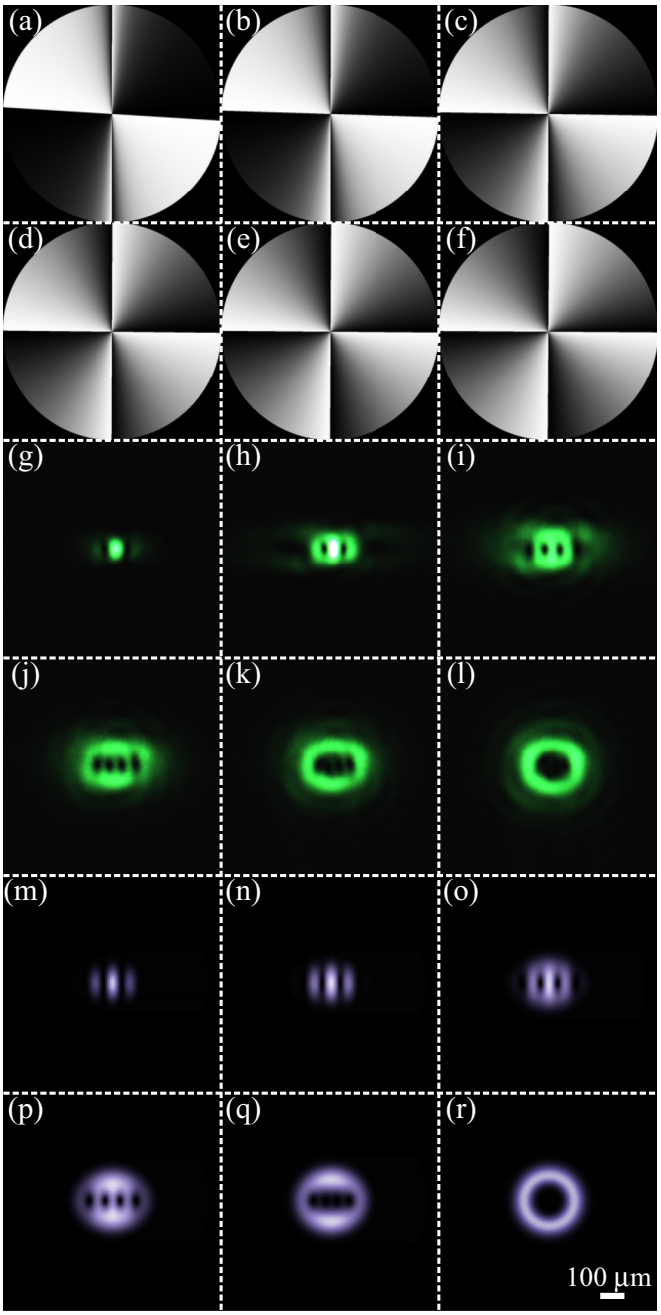

FIG. 5. (a)–(f) Phase functions of the elements; (g)–(l) corresponding experimental intensity distributions; and (m–r) computed intensity distributions in the focus of lens L_4 when using a SPP with $n = 4$ and with the ratio β taking values of 0.1 (a), (g), (m); 0.2 (b), (h), (n); 0.4 (c), (i), (o); 0.6 (d), (j), (p); 0.8 (e), (k), (q); and 1.0 (f), (l), (r). The intensity patterns are 900 μm × 900 μm in size.

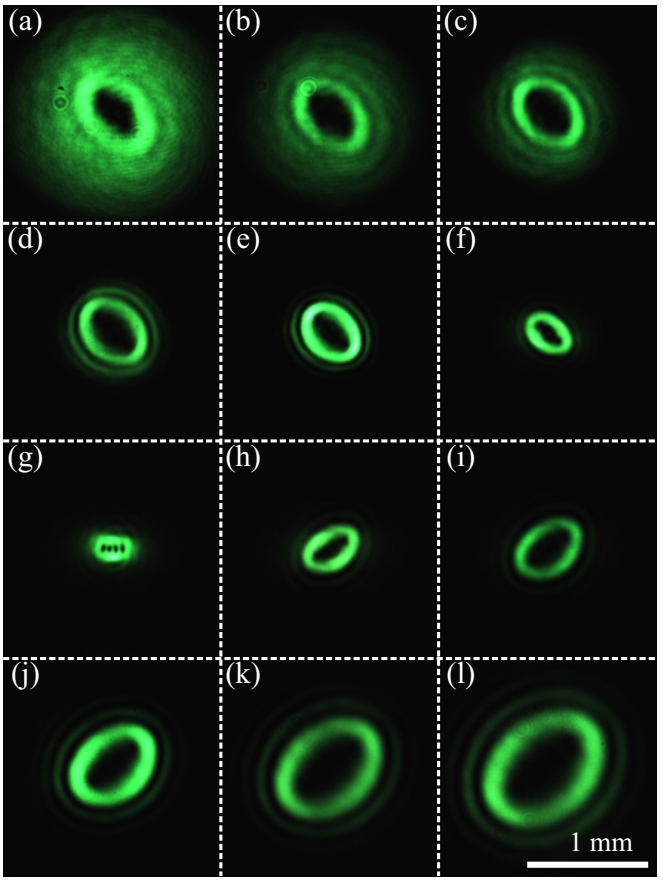

FIG. 6. Intensity patterns generated at different distances from the lens L_4 ($f_4 = 250$ mm) when using an elliptic SPP with $n = 4$ and $\beta = 0.6$: (a) 100 mm, (b) 125 mm, (c) 150 mm, (d) 175 mm, (e) 200 mm, (f) 225 mm, (g) 250 mm (focus), (h) 275 mm, (i) 300 mm, (j) 325 mm, (k) 350 mm, and (l) 375 mm. The intensity patterns are 1800 μm × 1800 μm in size.

intensity null at the Gaussian beam's center have been deduced. The EGV has been shown to carry a fractional OAM whose maximal value is equal to the vortex topological charge n attained at zero ellipticity of the vortex. The major axis of the intensity ellipse has been found to rotate, making an angle of 90° while propagating from the initial plane to the focal plane of a spherical lens. There are n intensity nulls on the major axis of the intensity ellipse, with the spacing between them varying both during propagation of the EGV and with varying ellipticity. The internull spacing is maximal in the focal plane, given the same ellipticity. When ellipticity is zero, all nulls get merged into a single on-axis, n-times degenerate intensity null. Such a beam has been experimentally generated via illuminating a SPP by a conventional Gaussian beam. Although strictly speaking, the transmittance of such a SPP in (31) is different from the complex amplitude of an elliptic intensity null in (1), nonetheless experimental results are in qualitative agreement with theory. This can be explained by the fact that functions in (1) and (31) have the same phase distributions.

It is worth noting that if, on the contrary, we assume an elliptic Gaussian beam implanted with a conventional radially symmetric n-times degenerate intensity null at the Gaussian beam's center, such a beam has an integer OAM equal to the vortex's topological charge n whatever the Gaussian beam ellipticity.

The EGV beam considered here differs from the more complicated elliptical vortex laser modes, which also have a fractional OAM and which were investigated earlier: EB [11], IG [12], HIG [13], HLG [15], and Mathieu beams [16]. The main difference is that the EGV beam is not a mode and changes its shape on propagation. The EGV beam is closest to the noncanonical vortices [20], but there is no theory in Ref. [20].

ACKNOWLEDGMENTS

This work was partially funded by the Ministry of Education and Science of the Russian Federation, RF President's grants for support of leading scientific schools (Grant No. NSh-9498.2016.9), and Young Candidates of Science (Grant No. MK-2390.2017.2), as well as Russian Foundation for Basic Research (RFBR) Grants No. 15-07-01174, No. 15-47-02492, No. 16-29-11698, and No. 16-47-630483.

[1] A. Mair, A. Vaziri, G. Weihs, and A. Zeilinger, Entanglement of the orbital angular momentum states of photons, Nature (London) **412**, 313 (2001).

[2] A. Vaziri, G. Weihs, and A. Zeilinger, Superpositions of the orbital angular momentum for applications in quantum experiments, J. Opt. B: Quantum Semiclassical Opt. **4**, S47 (2002).

[3] Q. Chen, B. Shi, Y. Zhang, and G. Guo, Entanglement of the orbital angular momentum states of the photon pairs generated in a hot atomic ensemble, Phys. Rev. A **78**, 053810 (2008).

[4] V. V. Kotlyar, A. A. Kovalev, and A. P. Porfirev, Asymmetric Gaussian optical vortex, Opt. Lett. **42**, 139 (2017).

[5] V. V. Kotlyar, A. A. Kovalev, and V. A. Soifer, Asymmetric Bessel modes, Opt. Lett. **39**, 2395 (2014).

[6] A. A. Kovalev, V. V. Kotlyar, and A. P. Porfirev, Asymmetric Laguerre-Gaussian beams, Phys. Rev. A **93**, 063858 (2016).

[7] A. Kumar, P. Vaity, and R. P. Singh, Grafting the core asymmetry to lift the degeneracy of optical vortices, Opt. Express **19**, 6182 (2011).

[8] M. R. Dennis, Rows of optical vortices from elliptically perturbing a high-order beam, Opt. Lett. **31**, 1325 (2006).

[9] V. V. Kotlyar, S. N. Khonina, A. A. Almazov, V. A. Soifer, K. Jefimovs, and J. Turunen, Elliptic Laguerre-Gaussian beams, J. Opt. Soc. Am. A **23**, 43 (2006).

[10] V. V. Kotlyar, A. A. Kovalev, and A. P. Porfirev, Vortex Hermite-Gaussian laser beams, Opt. Lett. **40**, 701 (2015).

[11] M. A. Bandres and J. C. Gutierrez-Vega, Elliptical beams, Opt. Express **16**, 21087 (2008).

[12] M. A. Bandres and J. C. Gutierrez-Vega, Ince-Gaussian beams, Opt. Lett. **29**, 144 (2004).

[13] J. B. Bentley, J. A. Devies, M. A. Bandres, and J. C. Gutierrez-Vega, Generation of helical Ince-Gaussian beams with a liquid-crystal display, Opt. Lett. **31**, 649 (2006).

[14] S. Lopez-Aguayo and J. C. Gutierrez-Vega, Elliptical modulated self-trapped singular beams in nonlocal nonlinear media: Ellipticons, Opt. Express **15**, 18326 (2007).

[15] E. G. Abramochkin and V. G. Volostnikov, Generalized Gaussian beams, J. Opt. A: Pure Appl. Opt. **6**, S157 (2004).

[16] S. Chave-Cedra, M. J. Padgett, I. Alisson, G. H. C. New, J. C. Guttierrez-Vega, A. T. O'Neil, I. Mac Vicar, and J. Courtial, Holographic generation and orbital angular momentum of high-order Mathieu beams, J. Opt. B: Quant. Opt. **4**, S52 (2002).

[17] A. A. Kovalev and V. V. Kotlyar, Lommel modes, Opt. Commun. **338**, 117 (2015).

[18] M. Krenn, R. Fickler, M. Huber, R. Lapkiewicz, W. Plick, S. Ramelow, and A. Zeilinger, Entangled singularity patterns of photons in Ince-Gauss modes, Phys. Rev. A **87**, 012326 (2013).

[19] W. N. Plick, M. Krenn, R. Fickler, S. Ramelow, and A. Zeilinger, Quantum orbital angular momentum of elliptically symmetric light, Phys. Rev. A **87**, 033806 (2013).

[20] G. Molina-Terriza, J. Recolons, J. P. Torres, and L. Torner, Observation of the Dynamical Inversion of the Topological Charge of an Optical Vortex, Phys. Rev. Lett. **87**, 023902 (2001).

[21] S. S. R. Oemrawsingh, X. Ma, D. Voigt, A. Aiello, E. R. Eliel, G. W. 't Hooft, and J. P. Woerdman, Experimental Demonstration of Fractional Orbital Angular Momentum Entanglement of Two Photons, Phys. Rev. Lett. **95**, 240501 (2005).

[22] M. A. Bendres and J. C. Gutierrez-Vega, Ince-Gaussian modes of the paraxial wave equation and stable resonators, J. Opt. Soc. Am. A **21**, 873 (2004).

[23] W. Miller, Jr., *Symmetry and Separation of Variables* (Addison-Wesley, Reading, MA, 1977).

[24] L. Allen, M. W. Beijersbergen, R. J. C. Spreeuw, and J. P. Woerdman, Orbital angular momentum of light and the transformation of Laguerre-Gaussian laser modes, Phys. Rev. A **45**, 8185 (1992).

[25] A. P. Prudnikov, Y. A. Brychkov, and O. I. Marichev, *Integrals and Series, Special Functions* (Gordon and Breach, New York, 1981).

[26] V. V. Kotlyar and A. A. Kovalev, Hermite-Gaussian modal beams with orbital angular momentum, J. Opt. Soc. Am. A **31**, 274 (2014).